Chemical Science

ROYAL SOCIETY OF CHEMISTRY

EDGE ARTICLE

View Article Online
View Journal | View Issue

Cite this: *Chem. Sci.*, 2025, **16**, 18832

All publication charges for this article have been paid for by the Royal Society of Chemistry

Received 15th July 2025
Accepted 8th September 2025

DOI: 10.1039/d5sc05237h

rsc.li/chemical-science

Engineering β-sheet morphologies *via* metal cross-linking and side chain modifications

Eisuke Tsunekawa,[a] Takahiro Nakama,[a] Makoto Fujita *[abc] and Tomohisa Sawada *[d]

Natural and artificial β-sheet assemblies often form helical structures due to the inherent twisting of peptide strands, typically observable by AFM and TEM but rarely analysed with single crystal X-ray diffraction (SCD) due to structural disorder. This study overcame such challenges by periodically cross-linking peptide strands in β-sheet tapes *via* metal coordination, creating perfectly ordered helical structures suitable for SCD analysis. Side chain interactions were found to drive helical twisting, and adjusting side chain substituents enabled tuning of the helical morphology, including the formation of double helices. These findings open new possibilities in β-sheet assembly design, advancing peptide engineering.

Introduction

Both natural and artificial β-sheet assemblies often exhibit various helical morphologies on the submicron scale due to the inherent twisting of peptide strands[1] or the flexibility of β-sheet tapes.[2] These helical structures can typically be observed by atomic force microscopy (AFM) and transmission electron microscopy (TEM),[3] but precise molecular-level structural analysis[4] by single crystal X-ray diffraction (SCD) has rarely been applied.[5] This is because β-sheets, composed of peptide strands, frequently develop types of disorder[6]—such as mixed parallel/antiparallel arrangements and/or shearing (*i.e.*, residue slips along the N- to C-terminal backbone direction between adjacent β-strands)[1b]—that prevent obtaining suitable diffraction data for SCD analysis. In this study, we successfully constructed helical β-sheet tapes completely free of such heterogeneity by cross-linking *i* and *i* + 2 peptide strands[7] through metal coordination (Fig. 1a). Thanks to this non-disordered structure, we were able to observe infinite twisted β-sheet tapes *via* SCD analysis. Careful examination of these helical structures revealed that side chain interactions within or between peptide strands induce the helical twist. By modifying side chain substituents, we were able to tune the helical morphology and even generate a double helical β-sheet composed of two β-sheet tapes. While recent advancements in protein *de novo* design have enabled accurate prediction of α-helix structures,[8] the design and structural prediction of β-sheet assemblies remain largely unexplored. This study is thus anticipated to open new avenues in peptide engineering based on β-sheet assemblies.

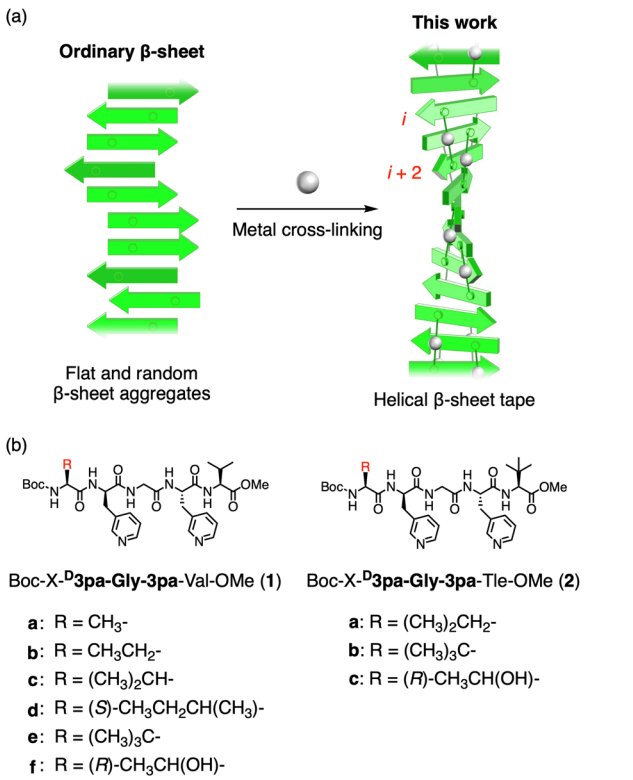

Fig. 1 (a) Schematic representation of this work. (b) Chemical structures of pentapeptides **1a–1f** and **2a–2c**.

[a]*Department of Applied Chemistry, School of Engineering, The University of Tokyo, Mitsui Link Lab Kashiwanoha 1, FS CREATION, 6-6-2 Kashiwanoha, Kashiwa, Chiba 277-0882, Japan*

[b]*Division of Advanced Molecular Science, Institute for Molecular Science, National Institutes of Natural Sciences, 5-1 Higashiyama, Myodaiji-cho, Okazaki, Aichi 444-8787, Japan*

[c]*Tokyo College, UT Institutes for Advanced Study (UTIAS), The University of Tokyo, Mitsui Link Lab Kashiwanoha 1, FS CREATION, 6-6-2 Kashiwanoha, Kashiwa, Chiba 277-0882, Japan. E-mail: mfujita@appchem.t.u-tokyo.ac.jp*

[d]*Laboratory for Chemistry and Life Science, Institute of Integrated Research, Institute of Science Tokyo, 4259 Nagatsuta, Midori-ku, Yokohama 226-8501, Japan. E-mail: sawada.t.ak@m.titech.ac.jp*

We recently reported that the coordination of pentapeptide **1a** with Ag^+ ions leads to the self-assembly of four-stranded β-sheet $[Ag_2(\mathbf{1a})_2]_2$ (**3**) with a [2]catenane topology consisting of two $Ag_2(\mathbf{1a})_2$ cyclic frameworks (Fig. 2a).[9] In the sequence of **1a**, the core sequence, –^{D}3pa-Gly-3pa– (where 3pa/^{D}3pa stand for β-(3-pyridyl)-L/D-alanine), contains two coordinating side chains (3-pyridylmethyl groups) oriented in opposite directions, enabling metal coordination to cross-link the *i* and *i* + 2 strands. In the crystalline state, the outer two strands (the first and fourth strands) are found to further form amide hydrogen bonds with adjacent four-stranded β-sheets, resulting in planar β-sheet tape structure $(\mathbf{3})_n$. Metal cross-linking from both sides of the β-sheet face, enabled by the incorporation of the D-amino acid residue, isolated β-sheet tapes from lamination, which

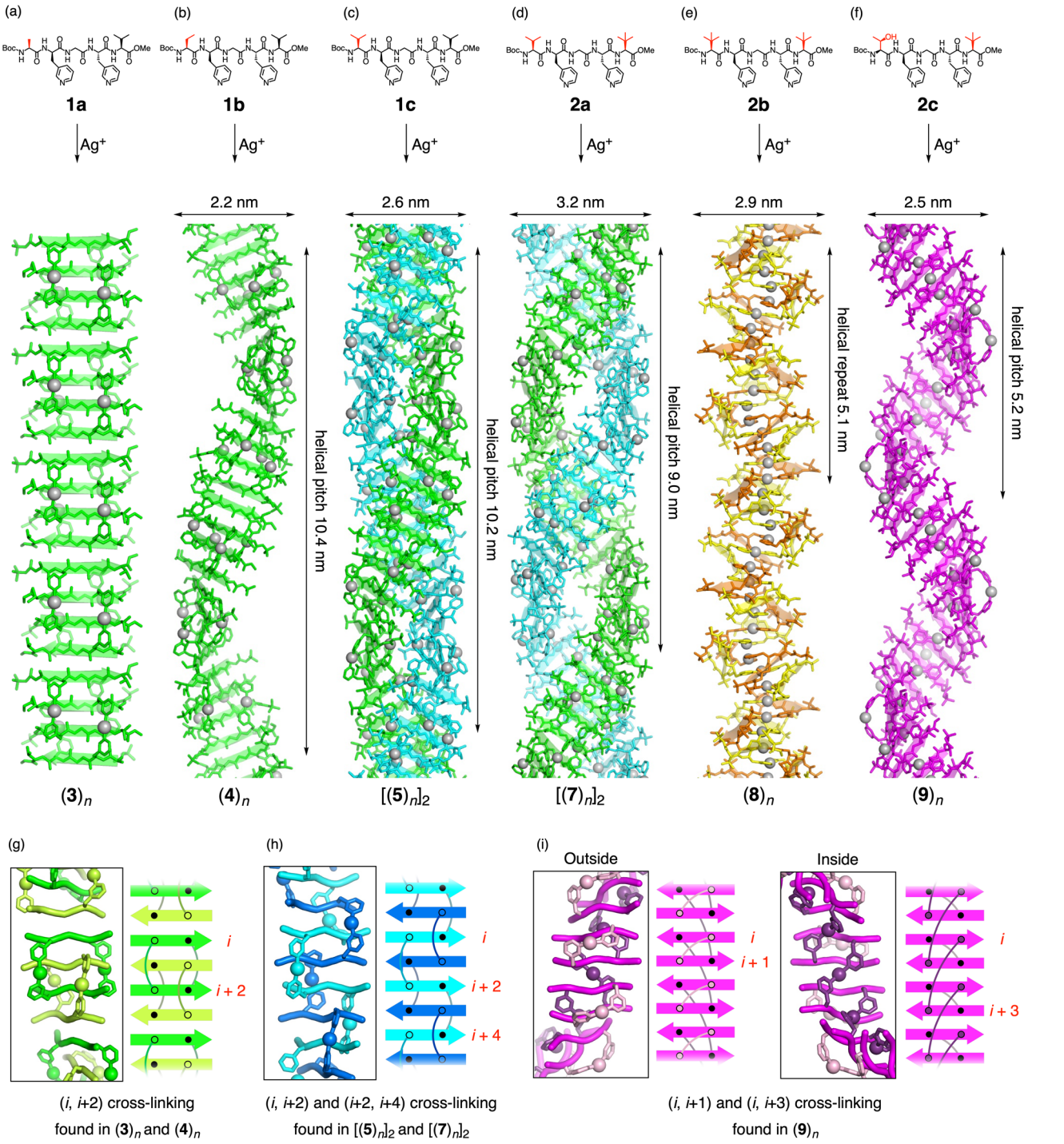

Fig. 2 Crystal structures of helical β-sheet tapes. (a–f) Side views of planar β-sheet tape $(\mathbf{3})_n$ from previous report[9] and helical structures for one pitch and (g–i) metal–peptide cross-linking manner observed. Structures are taken from (g) $(\mathbf{4})_n$, (h) $[(\mathbf{5})_n]_2$, and (i) $(\mathbf{9})_n$ as representatives.

exhibits potential for efficient helical induction. Here, we aim to investigate the relationship between the structure of the side chains on **1a** and the morphology of the resulting β-sheet tapes. Peptides **1b–1f** and **2a–2c** were synthesised where the side chain structure of the N- and/or C-terminal residues of **1a** were replaced with different residues (Fig. 1b, see also Experimental section in the SI and Fig. S1–S18). In contrast to many established pH-responsive β-sheet peptides governed by the interactions of charged side chains,[10] we chose non-charged side chains so as not to interfere the metal-crosslinking effect. The morphology of β-sheet tapes generated through Ag^+ coordination was studied by SCD analysis (Tables S1–S3 and Fig. S19–S37).

Results and discussion

Peptide **1b** with 2-aminobutyric acid (Abu) residues introduced at the N-terminal first residue (R = Et) and $AgNTf_2$ (0.25 μmol each) were mixed in $CHCl_3$/MeOH (1 : 1 (*v*/*v*), 50 μL), and slow vapor diffusion of ethyl acetate into this solution yielded colourless block crystals within three weeks (Fig. S19a). SCD analysis revealed that peptide **1b** self-assembled into in-register[11] antiparallel four-stranded β-sheet $[Ag_2(\mathbf{1b})_2]_2$ (**4**) with a catenated topology, similar to **3**, in which the *i* and *i* + 2 strands are cross-linked by Ag^+ coordination (Fig. 2g).

In the crystal structure, four-stranded β-sheet **4** is further assembled into β-sheet tape $(\mathbf{4})_n$ through hydrogen bonding of the outer strands, similar to $(\mathbf{3})_n$ (Fig. 2b). Interestingly, $(\mathbf{4})_n$ displayed a right-handed helical morphology with a helical pitch of 10.4 nm and a diameter of 2.2 nm. This long helical pitch consists of 24 β-strands, with half of them crystallographically independent (Fig. S20). The β-sheet tape was based on an in-register antiparallel β-sheet configuration at the hydrogen bonding sites (Fig. 3a). A top-down view (Fig. S37a) reveals the position of each residue within $(\mathbf{4})_n$ in the helical tape, showing that all ^{D}3pa side chains are positioned on the outer side of the helix, while all 3pa side chains are oriented inward. The alkyl side chain of the Abu and valine (Val) residues projects outward, contributing to the packing between helices. The C-terminal methyl ester also positions outward.

A superimposed view of each of the four-stranded β-sheet units, comprising flat $(\mathbf{3})_n$ and twisted $(\mathbf{4})_n$ structures, demonstrated that the twist originates from steric repulsion between the side chains (Fig. 3b). In the case of $(\mathbf{4})_n$, steric repulsion between the side chains of the Abu and ^{D}3pa residues causes the peptide structure around the N-terminus to distort more than in $(\mathbf{3})_n$ (Fig. 3b, left). This distortion leads to slight structural changes in the metal cross-linking, which propagated to form the helical morphology along the β-sheet axis.

Since it was confirmed that steric repulsion from the side chains of the Abu and ^{D}3pa residues induces strand twisting and the emergence of a helical morphology, we attempted complexation with Ag^+ using peptide ligands **1c–1e**, in which the Abu residue was replaced with bulkier Val, isoleucine (Ile), and *tert*-leucine (Tle) residues, respectively, to observe changes in the helical morphology. SCD analysis of the crystal formed through complexation of Ag^+ ions with ligand **1c** revealed the

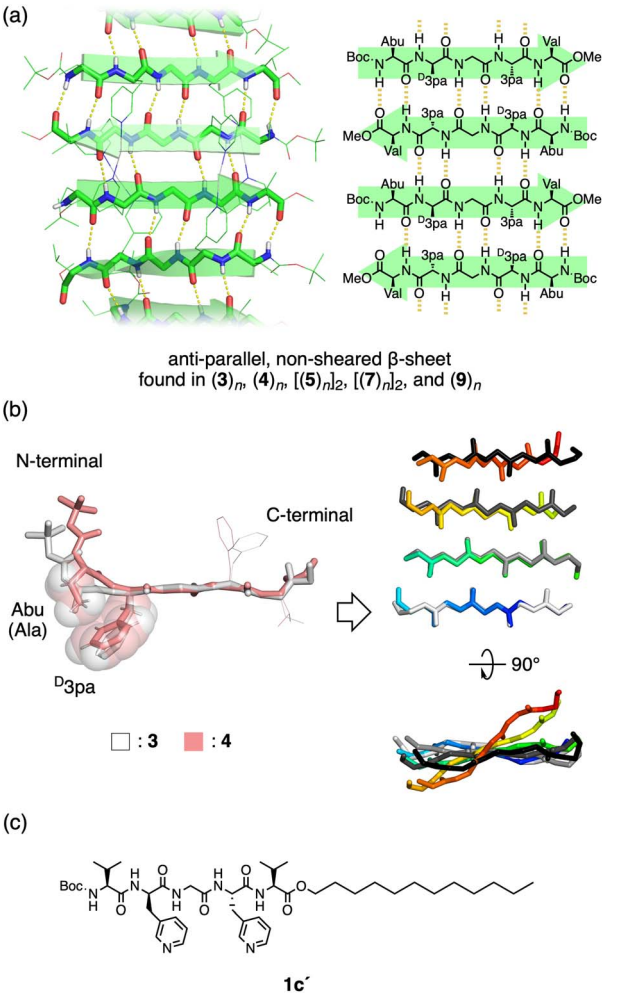

Fig. 3 Steric and hydrogen-bond interactions that control the β-sheet morphologies. (a) Local structure of the four-stranded β-sheet unit. Hydrogen bonds are shown as yellow dashed lines. (b) Overlaid structure of **3** and **4**. Comparison of conformation of single peptide (left). Side chains of Abu and ^{D}3pa residues are highlighted in translucent sphere. Main chain in four-stranded β-sheets (right) **3** (black and white) and **4** (rainbow). (c) Chemical structure of **1c′**.

formation of a helical β-sheet tape structure, $(Ag{\cdot}\mathbf{1c})_n$ ($(\mathbf{5})_n$), similar to $(\mathbf{4})_n$ (Fig. S21). Unexpectedly, it was found that this helical tape $(\mathbf{5})_n$ forms a double helix, $[(\mathbf{5})_n]_2$, by intertwining of two tapes (Fig. 2c). Although the helical structure of $(\mathbf{5})_n$ resembled that of $(\mathbf{4})_n$, the metal–peptide binding pattern differed. The cross-linking between the *i* and *i* + 2 strands did not give a discrete [2]catenane framework; instead, *i* + 2 linked with *i* + 4 through another 3-pyridylmethyl group within the strand, forming a coordination polymer (Fig. 2h). This change to more uniform cross-linking mode enabled packing into the duplex where interactions between two tapes consisted primarily of packing of ^{D}3pa residues and counter anions. In addition, the Boc group in $(\mathbf{5})_n$ is oriented deeper towards the interior of the double helix than that in $(\mathbf{4})_n$ (Fig. S37b). The helix of $(\mathbf{5})_n$ twists in a right-handed direction, with a pitch and diameter of 10.2 nm and 2.6 nm, respectively, and is slightly more tightly wound compared to $(\mathbf{4})_n$. Similar double helical

topology, $[(Ag\cdot\mathbf{1d})_n]_2$ ($[(\mathbf{6})_n]_2$, Fig. S38a and b), was observed in the Ag^+ complex of **1d**.

Ligand **1c′**, with a dodecyl group at the C-terminus of **1c**, formed a single helical tape $(\mathbf{5}')_n$ similar to $(\mathbf{4})_n$ (Fig. 3c and S39). This structure is suggestive. First, $(\mathbf{5}')_n$ is composed of a catenane unit, supporting the fact that the structures of the single and double helical tape(s) are generated from catenaned and polymeric modes, respectively (Fig. S40). Furthermore, $Ag_3(\mathbf{1c}')_4$ unit, which lacked one Ag^+ ion, co-existed in the structure of $(\mathbf{5}')_n$ (Fig. S39c and d). Thus, as a possible mechanism for the β-sheet tape formation, three β-strands first assemble at the nucleation step, and when the fourth β-strand join them, either pathway of the catenated or polymeric mode is selected for propagation (Fig. S41).

For ligand **1c**, we obtained a single crystal without metal complexation. In this case, the observed structure was a flat β-sheet with mixed orientation (Fig. S29e and f). This fact suggests that the steric repulsion of the side chains leads to the helix induction when the metal cross-linking suppresses strands' shearing and aligns the strands' orientations.

To investigate the effect of the fifth residue and to achieve better crystal quality for the following investigation, the C-terminal Val in **1c** was replaced with Tle (**2a**). Complexation with $AgNTf_2$ also showed double helical structure $[(7)_n]_2$ (Fig. 2d), with the same manner of the β-sheet pattern and metal–peptide linkages as $[(\mathbf{5})_n]_2$ (Fig. S29c and S38c). The crystal structure of $[(7)_n]_2$ was a relatively squashed duplex (helical pitch: 9.0 nm, diameter: 3.2 nm) with larger inner cavity (Fig. S37d). This result indicates that the introduction of Tle at the fifth residue does not significantly affect the metal–peptide linkage or the duplex formation. Overlaying each strand in double helices $[(\mathbf{5})_n]_2$ and $[(7)_n]_2$ showed only slight differences in twist (Fig. S42), and such slight differences were found to alter the helical parameters of pitch and width of β-sheet tapes. Inside $[(7)_n]_2$, even less inter-helical contacts existed those in $[(\mathbf{5})_n]_2$ (Fig. S43). This indicates the double helix formation was prompted by packing effects rather than attractive interactions as in DNA.

Regarding these insights, peptide **2b** was used instead of **1e**, since the diffraction intensity of the obtained crystal from **1e** was insufficient. In this case, the steric hindrance between residues became too large, making it difficult to adopt a β-sheet tape aggregation. Instead, complex helical structure $(Ag\cdot\mathbf{2b})_n$ ($(\mathbf{8})_n$) containing bulged[12] dimer unit $(\mathbf{2b})_2$, is generated (Fig. 4),

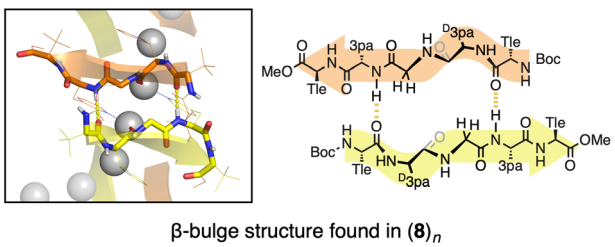

Fig. 4 Close up views of amide hydrogen-bonding pattern (yellow dashed lines) in $(\mathbf{8})_n$.

in which Ag^+ ions are helically surrounded by the β-bulged dimer units (Fig. 2e), forming a one-dimensional chain, $(Ag^+)_n$ (further structural details are described in the SI and Fig. S44).

Finally, we show the results of complex formation with Ag^+ for ligands **1f** and **2c**, in which a threonine (Thr) residue was introduced at the N-terminal first residue. Such a hydrophilic residue was chosen for wider scope of peptides without precluding the metal cross-linking. Unfortunately, no crystal suitable for SCD analysis was obtained from **1f**, but from **2c**, a left-handed single helical structure, $(Ag\cdot\mathbf{2c})_n$ ($(\mathbf{9})_n$), opposite to $(\mathbf{4})_n$–$(7)_n$, was observed (Fig. 2f). The helical pitch measures 5.2 nm, which is half the pitch length of $(\mathbf{4})_n$ or $(\mathbf{5})_n$, and it is composed of 16 peptide strands. Crystallographically, only two independent peptide strands exist, making it a more uniform helical structure (Fig. S25). The cross-linking mode of the metal–peptide complex differs significantly from that of helical β-sheet tapes $(\mathbf{4})_n$–$(7)_n$, with distinct binding modes observed on the inner and outer sides of the helix (Fig. 2i). On the outer side, adjacent i and $i+1$ strands are cross-linked, while on the inner side, i and $i+3$ strands are cross-linked, forming a β-sheet helical tape. This unique binding mode is stabilised by weak coordination of C=O···Ag^+ within the main chain (Fig. S45). We presume the hydroxy group of the Thr residue interacted with the main chain of the neighbouring strand *via* hydrogen bonding as a reason for such a unique helical morphology, distinctly different from those of $(\mathbf{4})_n$–$(7)_n$ (Fig. S46).

Conclusions

In summary, through the folding and assembly of pentapeptides with metal ions,[13] we successfully constructed helical β-sheet tapes with precise single-crystal structures. The β-sheet tape cross-linked with Ag^+ ions at the core sequence –^{D}3pa-Gly-3pa–adopted four types of helical assemblies depending on the bulkiness and interactions of the terminal side chains. Generally, even for synthetic helical structures constructed with reversible bonds, obtaining structures with atomic precision remains difficult.[5,14] Therefore, β-sheet tapes, with their diverse structural modes and intense aggregation characteristics, are extremely challenging targets for precise construction to a defined helical structure at the molecular level. Decades of studies in β-sheets from the viewpoint of molecular structures also report various factors contributing to the twisting of β-sheets,[3] making it difficult to design from scratch. However, by introducing metal–peptide cross-linking within a simple system using short β-sheet-forming peptides, we were able to reduce the complexity to a simple factor, steric effects of aliphatic side chains. While many β-sheet-based helical structures exhibit pronounced polymorphism in fibrillisation,[15] the process of folding and assembly based on reversible metal coordination bonding and the flexibility of short peptides produced a thermodynamically stable structure, enabling single-crystal formation. Crystallisation of short β-sheet-forming peptides often results in planar β-sheets due to the lamination of β-sheet layers.[16] However, such lamination was prevented for metal cross-linked β-sheets and facilitated helical induction in high efficiency. In addition, incorporation of a D-residue may have

another effect to induce a bent conformation, as seen in β-sheet-forming L/D-alternating cyclic peptides.[17] Careful examination of the D-residue at different positions is needed in the future. We believe that such atomic-level structure analysis contributes to the rational understanding and design of β-sheet helical morphologies.

Author contributions

T. S. devised the concept. E. T. and T. S. planned the experiments. E. T. performed the experiments. E. T., T. N., T. S., and M. F. analysed the data. E. T. wrote the initial manuscript. T. S. and M. F. revised the manuscript. T. S. and M. F. supervised the research project.

Conflicts of interest

There are no conflicts to declare.

Data availability

CCDC 2420304–2420311 contain the supplementary crystallographic data for this paper.[18a–h]

Synthetic procedures, NMR spectra and characterisation data for all new compounds and X-ray crystallographic data are available within this article and in the SI. Supplementary information is available. See DOI: **https://doi.org/10.1039/d5sc05237h**.

Acknowledgements

This work was supported by JSPS Grants-in-Aid for Specially Promoted Research (JP19H05461 to M. F.), Scientific Research (B) (JP24K01465 to T. S.) and Early-Career Scientists (JP21K14640 to T. N.), and by JST PRESTO (JPMJPR20A7 to T. S.), Japan. E. T. acknowledges a JSPS Research Fellowship for Young Scientists. The synchrotron X-ray crystallography was performed at the BL26B1 (2021B1246, 2022B1190, 2022B1308, 2024A1123) and BL41XU (2023A2546, 2024B2545) beamline at SPring-8. We thank Mr Satoshi Yoshida for supporting the synchrotron measurement at BL41XU.

Notes and references

1 (*a*) C. Chothia, *J. Mol. Biol.*, 1973, **75**, 295–302; (*b*) B. K. Ho and P. M. G. Curmi, *J. Mol. Biol.*, 2002, **317**, 291–308; (*c*) K. Fujiwara, S. Ebisawa, Y. Watanabe, H. Toda and M. Ikeguchi, *Proteins*, 2014, **82**, 1484–1493.

2 (*a*) A. Aggeli, I. A. Nyrkova, M. Bell, R. Harding, L. Carrick, T. C. B. McLeish, A. N. Semenov and N. Boden, *Proc. Natl. Acad. Sci. U. S. A.*, 2001, **98**, 11857–11862; (*b*) E. G. Emberly, R. Mukhopadhyay, C. Tang and N. S. Wingreen, *Proteins, Bioinf.*, 2004, **55**, 91–98.

3 (*a*) K. Makabe, D. McElheny, V. Tereshko, A. Hilyard, G. Gawlak, S. Yan, A. Koide and S. Koide, *Proc. Natl. Acad. Sci. U. S. A.*, 2006, **103**, 17753–17758; (*b*) V. Castelletto, I. W. Hamley, R. A. Hule and D. Pochan, *Angew. Chem., Int. Ed.*, 2009, **48**, 2317–2320; (*c*) Y. Hu, R. Lin, P. Zhang, J. Fern, A. G. Cheetham, K. Patel, R. Schulman, C. Kan and H. Cui, *ACS Nano*, 2016, **10**, 880–888; (*d*) M. Wang, J. Wang, P. Zhou, J. Deng, Y. Zhao, Y. Sun, W. Yang, D. Wang, Z. Li, X. Hu, S. M. King, S. E. Rogers, H. Cox, T. A. Waigh, J. Yang, J. R. Lu and H. Xu, *Nat. Commun.*, 2018, **9**, 5118; (*e*) C. W. G. Fishwick, A. J. Beevers, L. M. Carrick, C. D. Whitehouse, A. Aggeli and N. Boden, *Nano Lett.*, 2003, **3**, 1475–1479; (*f*) H. Cui, T. Muraoka, A. G. Cheetham and S. I. Stupp, *Nano Lett.*, 2009, **9**, 945–951.

4 F. Wang, O. Gnewou, A. Solemanifar, V. P. Conticello and E. H. Egelman, *Chem. Rev.*, 2022, **122**, 14055–14065.

5 Q. Zhang, R. Toyoda, L. Pfeifer and B. L. Feringa, *J. Am. Chem. Soc.*, 2023, **145**, 6976–6985.

6 (*a*) A. S. Robang, K. M. Wong, J. Leisen, R. Liu, W. L. Radford, T. R. Sudarshan, G. A. Hudalla and A. K. Paravastu, *J. Phys. Chem. B*, 2024, **128**, 5387–5396; (*b*) K. M. Wong, Y. Wang, D. T. Seroski, G. E. Larkin, A. K. Mehta, G. A. Hudalla, C. K. Hall and A. K. Paravastu, *Nanoscale*, 2020, **12**, 4506–4518.

7 The order of each strand lined up in a β-sheet is defined as *i*-th here.

8 J. L. Beesley and D. N. Woolfson, *Curr. Opin. Biotechnol.*, 2019, **58**, 175–182.

9 E. Tsunekawa, M. Fujita and T. Sawada, *Angew. Chem., Int. Ed.*, 2025, **64**, e202416442.

10 A. Aggeli, M. Bell, L. M. Carrick, C. W. G. Fishwick, R. Harding, P. J. Mawer, S. E. Radford, A. E. Strong and N. Boden, *J. Am. Chem. Soc.*, 2003, **125**, 9619–9628.

11 T. L. S. Benzinger, D. M. Gregory, T. S. Burkoth, H. Miller-Auer, D. G. Lynn, R. E. Botto and S. C. Meredith, *Proc. Natl. Acad. Sci. U. S. A.*, 1998, **95**, 13407–13412.

12 P. Craveur, A. P. Joseph, J. Rebehmed and A. G. de Brevern, *Protein Sci.*, 2013, **22**, 1366–1378.

13 (*a*) T. Sawada and M. Fujita, *Chem*, 2020, **6**, 1861–1876; (*b*) E. Tsunekawa, Y. Otsubo, Y. Yamada, A. Ikeda, N. Adachi, M. Kawasaki, A. Takasu, S. Aramaki, T. Senda, S. Sato, S. Yoshida, M. Fujita and T. Sawada, *J. Am. Chem. Soc.*, 2023, **145**, 16160–16165.

14 E. Yashima, N. Ousaka, D. Taura, K. Shimomura, T. Ikai and K. Maeda, *Chem. Rev.*, 2016, **116**, 13752–13990.

15 (*a*) M. Fändrich, J. Meinhardt and N. Grigorieff, *Prion*, 2009, **3**, 89–93; (*b*) F. Wang, O. Gnewou, S. Wang, T. Osinski, X. Zuo, E. H. Egelman and V. P. Conticello, *Matter*, 2021, **4**, 3217–3231.

16 (*a*) R. Nelson, M. R. Sawaya, M. Balbirnie, A. Ø. Madsen, C. Riekel, R. Grothe and D. Eisenberg, *Nature*, 2005, **435**, 773–778; (*b*) P.-N. Cheng, J. D. Pham and J. S. Nowick, *J. Am. Chem. Soc.*, 2013, **135**, 5477–5492; (*c*) A. J. Kuhn, B. Ehlke, T. C. Johnstone, S. R. J. Oliver and J. A. Raskatov, *Chem. Sci.*, 2022, **13**, 671–680.

17 R. Chapman, M. Danial, M. L. Koh, K. A. Jolliffe and S. Perrier, *Chem. Soc. Rev.*, 2012, **41**, 6023–6041.

18 (*a*) E. Tsunekawa, T. Nakama, M. Fujita and T. Sawada, CCDC 2420304: Experimental Crystal Structure Determination, 2025, DOI: **10.5517/ccdc.csd.cc2m7jbr**.; (*b*) E. Tsunekawa, T. Nakama, M. Fujita and T. Sawada, CCDC

2420305: Experimental Crystal Structure Determination, 2025, DOI: 10.5517/ccdc.csd.cc2m7jcs; (*c*) E. Tsunekawa, T. Nakama, M. Fujita and T. Sawada, CCDC 2420306: Experimental Crystal Structure Determination, 2025, DOI: 10.5517/ccdc.csd.cc2m7jdt; (*d*) E. Tsunekawa, T. Nakama, M. Fujita and T. Sawada, CCDC 2420307: Experimental Crystal Structure Determination, 2025, DOI: 10.5517/ccdc.csd.cc2m7jfv; (*e*) E. Tsunekawa, T. Nakama, M. Fujita and T. Sawada, CCDC 2420308: Experimental Crystal Structure Determination, 2025, DOI: 10.5517/ccdc.csd.cc2m7jgw; (*f*) E. Tsunekawa, T. Nakama, M. Fujita and T. Sawada, CCDC 2420309: Experimental Crystal Structure Determination, 2025, DOI: 10.5517/ccdc.csd.cc2m7jhx; (*g*) E. Tsunekawa, T. Nakama, M. Fujita and T. Sawada, CCDC 2420310: Experimental Crystal Structure Determination, 2025, DOI: 10.5517/ccdc.csd.cc2m7jjy; (*h*) E. Tsunekawa, T. Nakama, M. Fujita and T. Sawada, CCDC 2420311: Experimental Crystal Structure Determination, 2025, DOI: 10.5517/ccdc.csd.cc2m7jkz.